

## Application of Doppler backscattering diagnostics for studying edge localized modes on the Globus-M2 tokamak

© A.Yu. Tokarev<sup>1</sup>, A.Yu. Yashin<sup>1,2</sup>, N.S. Zhiltsov<sup>1,2</sup>, G.S. Kurskiev<sup>2</sup>, V.B. Minaev<sup>2</sup>,  
Yu.V. Petrov<sup>2</sup>, A.M. Ponomarenko<sup>1</sup>, N.V. Sakharov<sup>2</sup>

<sup>1</sup> Peter the Great Saint-Petersburg Polytechnic University, St. Petersburg, Russia

<sup>2</sup> Ioffe Institute, St. Petersburg, Russia

E-mail: tokarev\_ayu@spbstu.ru

Received May 3, 2024

Revised September 2, 2024 Accepted October 30, 2024

In the high confinement mode with an edge transport barrier (H-mode), large pressure gradients at the plasma periphery are observed, which leads to the appearance of edge localized modes (ELMs). On the spherical tokamak Globus-M2 ELMs can be divided into 2 types: synchronized with sawtooth oscillations in the center of the plasma and independent of them or desynchronized. In this paper, we present a study of synchronized edge localized modes by Doppler backscattering diagnostics. It is shown that the turbulence level changes dramatically during ELMs. In addition, the radial electric field profiles were constructed for synchronized edge localized modes of different amplitude.

**Keywords:** Tokamak, Doppler backscattering, edge localized modes.

DOI: 10.61011/TPL.2024.12.60377.6593k

At present, the main operation mode of tokamaks is the high confinement mode (H-mode) [1]. Confinement is improved due to the development of a region with strongly suppressed transport of particles and energy (a transport barrier) at the periphery of the plasma, which leads to the formation of a pedestal [2]. Large pressure gradients established in the pedestal are a potential source of plasma instabilities [3] (in particular, edge localized modes, ELMs) [4]. They cause periodic pulsed emissions of particles and energy from plasma onto the first wall and the divertor plates, which may get damaged [5]. Thus, the study of ELMs is highly relevant at present.

The peeling-ballooning mode model is used to characterize edge localized modes. Two factors triggering ELMs are distinguished in this model: the pressure gradient from the low field side field (ballooning mode) and the current flowing near the separatrix (peeling mode) [6]. More than five types of edge localized modes differing in size and degree of their influence on plasma confinement are distinguished, but types I, II, and III are the most common. With rare exceptions, only type III/V modes are observed at spherical tokamaks [7].

Edge localized modes at the Globus-M2 spherical tokamak differ somewhat from the generally accepted classification. In addition to the standard (desynchronized) type III/V ELMs occurring spontaneously in the high confinement mode [8], edge localized modes synchronized with sawtooth oscillations are observed on the Globus-M2 tokamak in the center of the plasma [9]. They are being studied actively at the Globus-M2 tokamak.

A wide variety of diagnostics are suitable for ELM investigation. From the very beginning, the  $D_\alpha$  line emission diagnostics, which allows to observe particle and energy

fluxes from plasma, has been used for their detection. However, data from the confinement region are the most valuable. Such data are provided by Doppler backscattering (DBS) diagnostics [10], which has been used successfully to study ELMs at the Globus-M2 tokamak [11]. In the present study, we report the results of measurement of the velocity of plasma rotation perpendicular to the magnetic field, which were used to calculate the radial electric field, during synchronized ELMs at the Globus-M2 spherical tokamak. The first results of the study of desynchronized ELMs have been reported recently in [12].

The Globus-M2 spherical tokamak has major radius  $R = 0.36$  m, minor radius  $a = 0.24$  m, and aspect ratio  $R/a = 1.5$ . The design values of the toroidal magnetic field and the plasma current are as high as 1 T and 0.5 MA, respectively [13]. The triangularity and elongation of the plasma column may reach 0.5 and 2.2, respectively. In the analyzed discharge, transition to the high confinement mode due to neutral beam co-injection (NBI) with a power up to 1 MW. The average electron density increases to  $\langle n_e \rangle \sim 1 \cdot 10^{20} \text{ m}^{-3}$ .

It is in the high confinement mode that edge localized modes synchronized with sawtooth oscillations are observed. Figure 1 shows the parameters of analysed discharge #41152. Plasma is in the high confinement mode. The average electron density is presented in Fig. 1, *a*. The dotted curve in Fig. 1, *b* represents the diagnostic signal of the intensity of collimated soft X-ray radiation along the chord directed at the center of the column. Sawtooth oscillations are seen clearly in this signal. The solid curve in Fig. 1, *b* represents the  $D_\alpha$  line emission diagnostic signal with periodic bursts that correspond to ELMs. It can be seen that the  $D_\alpha$  diagnostic signal bursts occur immediately after a sharp reduction in the soft X-ray intensity. This is a

characteristic sign of the development of synchronized edge localized modes.

The Doppler backscattering diagnostics, which has been proven efficient at a number of tokamaks around the world, was used to study ELMs [14–17]. It involves the detection of electromagnetic radiation backscattered off density fluctuations near the cutoff of the probing beam with a given frequency. Since the density fluctuations are extended along the magnetic field lines, they effectively form a diffraction grating. Due to the movement of fluctuations, the diffraction grating rotates around the plasma column. The amplitude of scattered electromagnetic radiation is directly proportional to the magnitude of fluctuations of electron density with a certain value of the wave vector  $k_{\perp}$ . Typical wave vector values for fluctuations recorded in the discussed experiments are  $k_{\perp} = 2.7\text{--}11.6\text{ cm}^{-1}$ . The phase contains a Doppler shift due to the rotation of fluctuations together with plasma. This allows one to determine the rotation velocity of plasma in crossed electric and magnetic fields and, consequently, the radial electric field under the assumption of smallness of the phase velocity of propagation of fluctuations. A more detailed description of Doppler backscattering diagnostics was provided in [14].

The use of several probing frequencies makes the DBS study of plasma much simpler, since simultaneous measurements at different distances from the center of the plasma column become possible. This makes it possible to examine the radial dependence of plasma parameters. Therefore, the Globus-M2 tokamak uses two multi-frequency systems. The first allows one to probe plasma at four frequencies: 20, 29, 39, and 48 GHz [18]. This corresponds to edge region  $0.8 < \rho < 1.1$ . The second system has six frequency channels: 50–70 GHz in 5 GHz increments [10]. This provides an opportunity to examine inner plasma regions  $0.4 < \rho < 0.8$ . The use of these two systems at the Globus-M2 tokamak allowed us to study in detail the process of transition to the classical high confinement mode (H-mode) [19] and the high confinement mode without ELMs (ELM-free H-mode) [20], as well as such plasma oscillatory processes as limit cycle oscillations [21,22], the geodetic acoustic mode [23,24], Alfvén modes [25,26], quasi-coherent modes [27], tearing modes [28], and the formation of plasma filaments [29,30], which, as revealed by full-wave modeling [31,32], may affect significantly the Doppler backscattering spectrum [33].

The result of operation of the DBS system at the Globus-M2 tokamak are digitized signals in ten channels with different sampling rates. Each channel has two signals:  $I$  (initial) and  $Q$  (phase-shifted by  $\pi/2$ ). When data are processed, individual signals are immediately converted into complex channels. The amplitude of a complex signal is proportional to the amplitude of fluctuations at which scattering occurred. The derivative of the complex signal phase is proportional to the Doppler frequency shift, and the Doppler frequency shift is proportional to the plasma

drift velocity in the crossed radial electric and total magnetic fields.

Typical discharge #41152 with synchronized ELMs was chosen for analysis. The data of  $D_{\alpha}$  emission diagnostics during the bursts of synchronized edge localized modes and the processed signals of Doppler backscattering diagnostics are shown in Fig. 2. The  $D_{\alpha}$  diagnostic signal (Fig. 2, *a*) features periodic disturbances with a period of  $T \approx 4$  ms, which correspond to ELM bursts. The amplitude of the received DBS signal at a probing frequency of 50 GHz (panel *b*) and its Doppler shift (panel *c*) are also shown in Fig. 2. This channel corresponds to the position of the probing radiation cutoff at radius  $\rho \approx 0.8$  and cutoff density  $n_e \approx 3.1 \cdot 10^{19}\text{ m}^{-3}$ . This figure does not provide a clear indication of how the received signal amplitude behaves during a  $D_{\alpha}$  diagnostic signal burst, although it does increase noticeably within certain bursts. This increase in the DBS signal amplitude corresponds to an increase in the amplitude of density fluctuations, which scatter the probing signal more strongly. However, more obvious disturbances are also seen in the Doppler shift of the signal, which is proportional to the velocity of plasma rotation perpendicular to the total magnetic field (and, consequently, to the radial electric field). It can be seen from Fig. 2, *c* that the Doppler shift of the DBS signal (and, consequently, the plasma rotation velocity) remains virtually unchanged between bursts and does not exceed 100 kHz. The modulus of the Doppler shift of the signal increases significantly during ELMs and may reach a level of approximately 400 kHz. Thus, it can be stated that the DBS diagnostics is well-suited for examination of edge localized modes, since they alter both the modulus of the received diagnostic signal and (much more profoundly) the derivative of its phase.

To study radial electric field  $E_r$  during the bursts of edge localized modes, its values were first determined during ELMs of different sizes occurring at different moments in time in discharge #41152. The size was determined from the amplitude of the  $D_{\alpha}$  diagnostic signal burst during an ELM burst. Examples of „large“ bursts are shown in Figs. 1 and 2. During „small“ bursts, the amplitude of the  $D_{\alpha}$  emission diagnostic signal did not exceed 1.5 a.u.; in the case of „large“ bursts, the amplitude increased to 2.7 a.u. In addition, all synchronized ELMs investigated in the present study were observed in a single discharge #41152, but at different time points with the same signal normalization conditions.

The obtained results were averaged over similar events (the  $D_{\alpha}$  diagnostic signal was used for similarity assessment). The use of a multi-frequency system made it possible to construct a radial electric field profile in each specific case, which is demonstrated in Fig. 3 for discharge #41152. Figures 3, *a* and *b* present the profiles for „large“ and „small“ ELMs, respectively. The same scales were used in both cases. The  $D_{\alpha}$  and DBS diagnostic signals for „large“ ELMs are also shown in Fig. 2. The solid curve in Fig. 3 is the  $E_r$  profile between ELMs, while the dashed

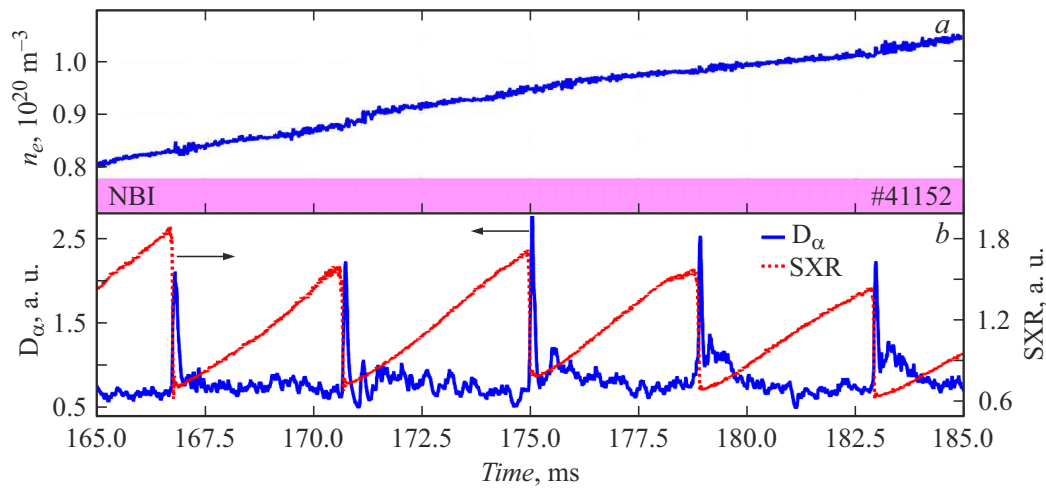


**Figure 1.** Temporal evolution of plasma parameters for discharge #41152. *a* — Average electron density; *b* — soft X-ray (SXR) intensity diagnostic signal and  $D_\alpha$  emission diagnostic signal. Plasma current  $I_p \approx 300$  kA and magnetic field  $B_T \approx 0.8$  T were maintained in this discharge.

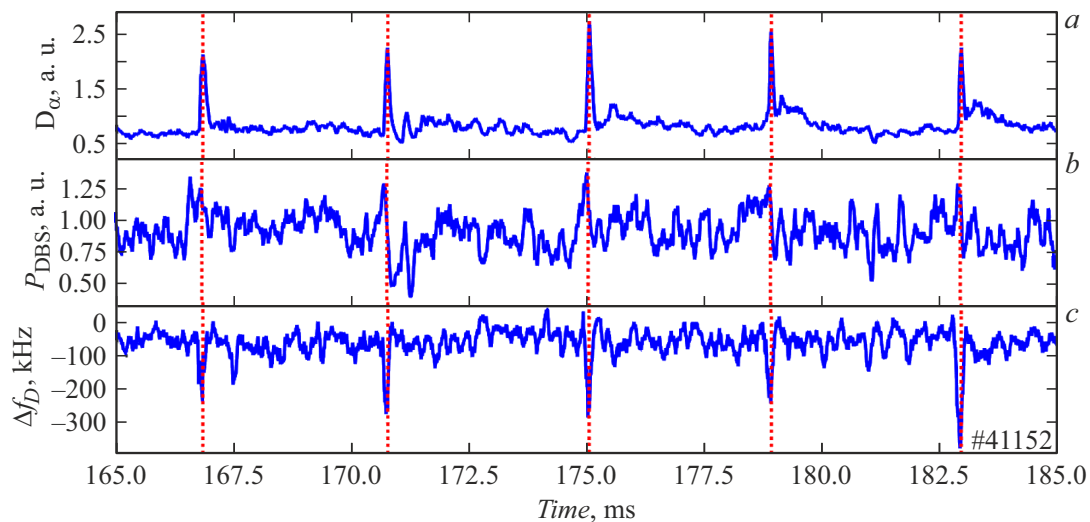


**Figure 2.** Temporal evolution of plasma parameters for discharge #41152 during synchronized ELMs. *a* —  $D_\alpha$  emission; *b* — amplitude of the received DBS signal at a probing frequency of 50 GHz; *c* — Doppler frequency shift of the received DBS signal at a probing frequency of 50 GHz.

curve corresponds to the maximum  $D_\alpha$  emission, which is associated with the ELM disruption peak. Let us first examine the profile in Fig. 3, *a*. It is evident that the radial electric field is weak between bursts (its modulus does not exceed 1 kV/m) and has a local maximum (in magnitude) near the separatrix. The field sign changes outside. Within the peak of  $D_\alpha$  emission, the electric field modulus increases synchronously at all radii up to 8 cm inside the separatrix. In the inner plasma region, an increase to 2 kV/m is seen. A local maximum of 3 kV/m is observed on the separatrix, which corresponds to a 4-fold field enhancement. In Fig. 3, *b*, the radial electric field behaves differently. First, the curves are almost indistinguishable: a 1.5–2-fold field variation is observed

inside the confinement region, while virtually no changes are seen near the separatrix. Second, the values of  $E_r$  both during „small“ ELMs and between them nearly match the value of  $E_r$  between „large“ ELM bursts. This indicates that „large“ ELMs strongly perturb plasma at all the studied radii, while „small“ ELMs have virtually no effect on the radial electric field.

Thus, it was demonstrated that Doppler backscattering diagnostics is a powerful instrument for examination of edge localized modes. ELMs alter profoundly the Doppler frequency shift of the received signal, although its amplitude behaves ambiguously. This was used to construct a profile of the radial electric field averaged over several events during edge localized modes synchronized with sawtooth

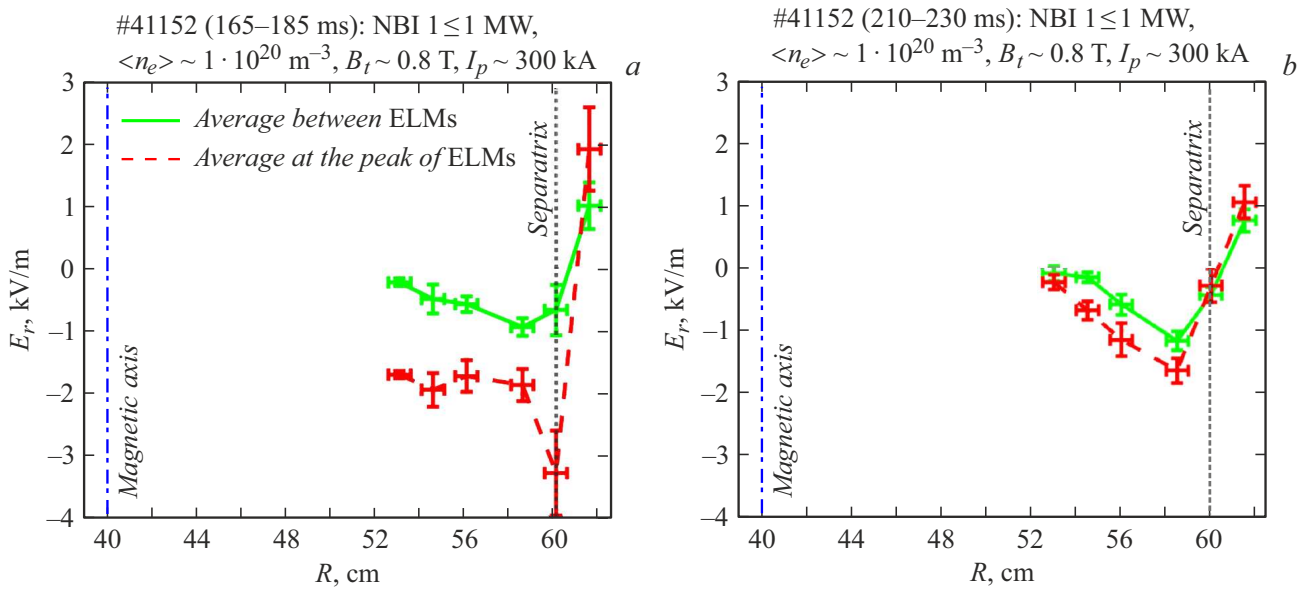


**Figure 3.** Averaged profiles of the radial electric field of discharge #41152. *a* — „Large“ ELMs; *b* — „small“ ELMs. The dashed and solid curves correspond to the average field value at the maxima of  $D_\alpha$  bursts and the average level between bursts, respectively.

oscillations at the Globus-M2 spherical tokamak. It was demonstrated that  $E_r$  increases noticeably (by a factor of 2–4) at all the examined radii during relatively „strong“ ELMs. This may be attributed to changes in the pressure gradient in the pedestal due to the profound influence of ELMs on plasma. Relatively „weak“ ELMs induce no noticeable changes in the field, and the obtained values are close to the radial electric field magnitude between „strong“ ELMs. This is presumably attributable to the weak influence of „small“ ELMs on plasma.

### Funding

This study was supported by grant No. 23-72-00024 (<https://rscf.ru/project/23-72-00024>) from the Russian Science Foundation. Experiments were carried out at the unique scientific facility Globus-M Spherical Tokamak, which is a part of the Federal Center for Collective Use „Materials Science and Diagnostics in Advanced Technologies“.

### Conflict of interest

The authors declare that they have no conflict of interest.

### References

- [1] F. Wagner, G. Becker, K. Behringer, D. Campbell, A. Eberhagen, W. Engelhardt, G. Fussmann, O. Gehre, J. Gernhardt, G. v. Gierke, G. Haas, M. Huang, F. Karger, M. Keilhacker, O. Klüber, M. Kornherr, K. Lackner, G. Lisitano, G.G. Lister, H.M. Mayer, D. Meisel, E.R. Müller, H. Murmann, H. Niedermeyer, W. Poschenrieder, H. Rapp, H. Röhr, F. Schneider, G. Siller, E. Speth, A. Stübler, K.H. Steuer, G. Venus, O. Vollmer, Z. Yü, Phys. Rev. Lett., **49** (19), 1408 (1982). DOI: 10.1103/PhysRevLett.49.1408
- [2] E.J. Doyle, W.A. Houlberg, Y. Kamada, V. Mukhovatov, T.H. Osborne, A. Polevoi, G. Bateman, J.W. Connor, J.G. Cordey, T. Fujita, X. Garbet, T.S. Hahm, L.D. Horton, A.E. Hubbard, F. Imbeaux, F. Jenko, J.E. Kinsey, Y. Kishimoto, J. Li, T.C. Luce, Y. Martin, M. Ossipenko, V. Parail, A. Peeters, T.L. Rhodes, J.E. Rice, C.M. Roach, V. Rozhansky, F. Ryter, G. Saibene, R. Sartori, A.C.C. Sips, J.A. Snipes, M. Sugihara, E.J. Synakowski, H. Takenaga, T. Takizuka, K. Thomsen, M.R. Wade, H.R. Wilson, ITPA Transport Physics Topical Group, ITPA Confinement Database and Modelling Topical Group and ITPA Pedestal and Edge Topical Group, Nucl. Fusion, **47** (6), S18 (2007). DOI: 10.1088/0029-5515/47/6/S02
- [3] T.C. Hender, J.C. Wesley, J. Bialek, A. Bondeson, A.H. Boozer, R.J. Buttery, A. Garofalo, T.P. Goodman, R.S. Granetz, Y. Gribov, O. Gruber, M. Gryaznevich, G. Giruzzi, S. Günter, N. Hayashi, P. Helander, C.C. Hegna, D.F. Howell, D.A. Humphreys, G.T.A. Huysmans, A.W. Hyatt, A. Isayama, S.C. Jardin, Y. Kawano, A. Kellman, C. Kessel, H.R. Koslowski, R.J. La Haye, E. Lazzaro, Y.Q. Liu, V. Lukash, J. Manickam, S. Medvedev, V. Mertens, S.V. Mirnov, Y. Nakamura, G. Navratil, M. Okabayashi, T. Ozeki, R. Paccagnella, G. Pautasso, F. Porcelli, V.D. Pustovitov, V. Riccardo, M. Sato, O. Sauter, M.J. Schaffer, M. Shimada, P. Sonato, E.J. Strait, M. Sugihara, M. Takechi, A.D. Turnbull, E. Westerhof, D.G. Whyte, R. Yoshino, H. Zohm and the ITPA MHD, Disruption and Magnetic Control Topical Group, Nucl. Fusion, **47** (6), S128 (2007). DOI: 10.1088/0029-5515/47/6/S03
- [4] J.W. Connor, Plasma. Phys. Control. Fusion, **40** (5), 531 (1998). DOI: 10.1088/0741-3335/40/5/002
- [5] J.W. Connor, A. Kirk, H.R. Wilson, AIP Conf. Proc., **1013** (1), 174 (2008). DOI: 10.1063/1.2939030

- [6] P.B. Snyder, H.R. Wilson, J.R. Ferron, L.L. Lao, A.W. Leonard, D. Mossessian, M. Murakami, T.H. Osborne, A.D. Turnbull, X.Q. Xu, Nucl. Fusion, **44** (2), 320 (2004). DOI: 10.1088/0029-5515/44/2/014
- [7] A.W. Leonard, Phys. Plasmas, **21** (9), 090501 (2014). DOI: 10.1063/1.4894742
- [8] V.V. Solokha, G.S. Kurskiev, A.Yu. Yashin, I.M. Balachenkov, V.I. Varfolomeev, A.V. Voronin, V.K. Gusev, V.Yu. Goryainov, V.V. Dyachenko, N.S. Zhiltsov, E.O. Kiselev, V.B. Minaev, A.N. Novokhatsky, Yu.V. Petrov, A.M. Ponomarenko, N.V. Sakharov, A.Yu. Telnova, E.E. Tkachenko, V.A. Tokarev, S.Yu. Tolstyakov, E.A. Tukhmeneva, N.A. Khromov, P.B. Shchegolev, Plasma Phys. Rep., **49** (4), 419 (2023). DOI: 10.1134/S1063780X23600184
- [9] V.V. Bulanin, G.S. Kurskiev, V.V. Solokha, A.Yu. Yashin, N.S. Zhiltsov, Plasma Phys. Control. Fusion, **63** (12), 122001 (2021). DOI: 10.1088/1361-6587/ac36a4
- [10] A.Y. Yashin, V.V. Bulanin, V.K. Gusev, V.B. Minaev, A.V. Petrov, Y.V. Petrov, A.M. Ponomarenko, V.I. Varfolomeev, JINST, **17** (1), C01023 (2022). DOI: 10.1088/1748-0221/17/01/C01023
- [11] A. Ponomarenko, V. Gusev, E. Kiselev, G. Kurskiev, V. Minaev, A. Petrov, Y. Petrov, N. Sakharov, V. Solokha, N. Teplova, P. Shchegolev, A. Yashin, N. Zhiltsov, Nucl. Fusion, **64** (2), 022001 (2024). DOI: 10.1088/1741-4326/ad0ead
- [12] A.Yu. Tokarev, A.Yu. Yashin, A.M. Ponomarenko, V.K. Gusev, N.S. Zhiltsov, G.S. Kurskiev, V.B. Minaev, Yu.V. Petrov, N.V. Sakharov, V.V. Solokha, V.A. Velizhanin, Plasma Phys. Rep., **50** (5), 541 (2024). DOI: 10.1134/S1063780X24600518
- [13] G.S. Kurskiev, N.V. Sakharov, V.K. Gusev, V.B. Minaev, I.V. Miroshnikov, Yu.V. Petrov, A.Yu. Telnova, N.N. Bakharev, E.O. Kiselev, N.S. Zhiltsov, P.B. Shchegolev, I.M. Balachenkov, V.I. Varfolomeev, A.V. Voronin, V.Yu. Goryainov, V.V. Dyachenko, E.G. Zhilin, M.V. Iliasova, A.A. Kavin, A.N. Kononov, S.V. Krikunov, K.M. Lobanov, A.D. Melnik, A.B. Mineev, A.N. Novokhatsky, M.I. Patrov, A.V. Petrov, A.M. Ponomarenko, O.M. Skrekel', V.A. Solovei, V.V. Solokha, E.E. Tkachenko, V.A. Tokarev, S.Yu. Tolstyakov, E.A. Tukhmeneva, E.M. Khilkevitch, N.A. Khromov, F.V. Chernyshev, A.E. Shevelov, K.D. Shulyat'ev, A.Yu. Yashin, Plasma Phys. Rep., **49** (4), 403 (2023). DOI: 10.1134/S1063780X23600214
- [14] G.D. Conway, J. Schirmer, S. Kluge, W. Suttrop, E. Holzhauser, the ASDEX Upgrade Team, Plasma Phys. Control. Fusion, **46** (6), 951 (2004). DOI: 10.1088/0741-3335/46/6/003
- [15] C. Silva, E.R. Solano, J.C. Hillesheim, E. Delabie, G. Birkenmeier, L. Gil, C. Giroud, R.B. Morales, D. Nina and JET Contributors, Nucl. Fusion, **62** (12), 126057 (2022). DOI: 10.1088/1741-4326/ac97f4
- [16] X. Feng, A.D. Liu, C. Zhou, M.Y. Wang, J. Zhang, Z.Y. Liu, Y. Liu, T.F. Zhou, S.B. Zhang, D.F. Kong, L.Q. Hu, J.X. Ji, H.R. Fan, H. Li, T. Lan, J.L. Xie, W.Z. Mao, Z.X. Liu, W.X. Ding, G. Zhuang, W.D. Liu, Rev. Sci. Instrum., **90** (2), 024704 (2019). DOI: 10.1063/1.5075615
- [17] Z. Shi, W. Zhong, M. Jiang, Z. Yang, B. Zhang, P. Shi, W. Chen, J. Wen, C. Chen, B. Fu, Z. Liu, X. Ding, Q. Yang, X. Duan, Rev. Sci. Instrum., **87** (11), 113501 (2016). DOI: 10.1063/1.4966680
- [18] V.V. Bulanin, A.Y. Yashin, A.V. Petrov, V.K. Gusev, V.B. Minaev, M.I. Patrov, Y.V. Petrov, D.V. Prisiazhniuk, V.I. Varfolomeev, Rev. Sci. Instrum., **92** (3), 033539 (2021). DOI: 10.1063/5.0030307
- [19] A. Ponomarenko, A. Yashin, G. Kurskiev, V. Minaev, A. Petrov, Y. Petrov, N. Sakharov, N. Zhiltsov, Sensors, **23** (2), 830 (2023). DOI: 10.3390/s23020830
- [20] A.Y. Yashin, V.V. Bulanin, A.V. Petrov, V.K. Gusev, G.S. Kurskiev, V.B. Minaev, M.I. Patrov, Yu.V. Petrov, Plasma Phys. Rep., **46** (7), 683 (2020). DOI: 10.1134/S1063780X20070107
- [21] A.Yu. Yashin, V.V. Bulanin, V.K. Gusev, G.S. Kurskiev, M.I. Patrov, A.V. Petrov, Yu.V. Petrov, S.Yu. Tolstyakov, Nucl. Fusion, **58** (11), 112009 (2018). DOI: 10.1088/1741-4326/aac4d8
- [22] O. Grover, P. Manz, A.Y. Yashin, D.I. Refy, J. Seidl, N. Vianello, G. Birkenmeier, E.R. Solano, M. Sos, P. Bohm, P. Bilkova, M. Hron, R. Panek, the ASDEX Upgrade Team, the COMPASS Team, the Globus-M Team, JET Contributors, Nucl. Fusion, **64** (2), 026001 (2024). DOI: 10.1088/1741-4326/ad0eae
- [23] A.Yu. Yashin, V.V. Bulanin, V.K. Gusev, N.A. Khromov, G.S. Kurskiev, V.B. Minaev, M.I. Patrov, A.V. Petrov, Yu.V. Petrov, D.V. Prisyazhnyuk, N.V. Sakharov, P.B. Shchegolev, S.Yu. Tolstyakov, V.I. Varfolomeev, F. Wagner, Nucl. Fusion, **54** (11), 114015 (2014). DOI: 10.1088/0029-5515/54/11/114015
- [24] V.V. Bulanin, F. Wagner, V.I. Varfolomeev, V.K. Gusev, G.S. Kurskiev, V.B. Minaev, M.I. Patrov, A.V. Petrov, Yu.V. Petrov, D.V. Prisyazhnyuk, N.V. Sakharov, S.Yu. Tolstyakov, N.A. Khromov, P.B. Shchegolev, A.Yu. Yashin, Tech. Phys. Lett., **40** (5), 375 (2014). DOI: 10.1134/S106378501405006X
- [25] V.V. Bulanin, N.N. Bakharev, V.K. Gusev, G.S. Kurskiev, V.B. Minaev, M.I. Patrov, A.V. Petrov, Yu.V. Petrov, N.V. Sakharov, P.B. Shchegolev, A.Yu. Telnova, S.Yu. Tolstyakov, A.Yu. Yashin, Phys. Atom. Nucl., **83** (7), 1124 (2020). DOI: 10.1134/S1063778820070042
- [26] V.V. Bulanin, I.M. Balachenkov, V.I. Varfolomeev, V.K. Gusev, G.S. Kurskiev, V.B. Minaev, M.I. Patrov, A.V. Petrov, Yu.V. Petrov, A.M. Ponomarenko, A.Yu. Telnova, P.B. Shchegolev, A.Yu. Yashin, Tech. Phys. Lett., **47** (2), 197 (2021). DOI: 10.1134/S1063785021020206
- [27] A.Yu. Yashin, V.V. Bulanin, V.K. Gusev, E.O. Kiselev, G.S. Kurskiev, V.B. Minaev, M.I. Patrov, A.V. Petrov, Yu.V. Petrov, A.M. Ponomarenko, P.B. Shchegolev, Nucl. Fusion, **61** (9), 092001 (2021). DOI: 10.1088/1741-4326/ac1297
- [28] A. Yashin, A. Ponomarenko, I. Balachenkov, G. Kurskiev, E. Kiselev, V. Minaev, A. Petrov, Y. Petrov, N. Sakharov, N. Zhiltsov, Appl. Sci., **13** (6), 3430 (2023). DOI: 10.3390/app13063430
- [29] V.V. Bulanin, V.K. Gusev, N.A. Khromov, G.S. Kurskiev, V.B. Minaev, M.I. Patrov, A.V. Petrov, M.A. Petrov, Yu.V. Petrov, D. Prisiazhniuk, N.V. Sakharov, S.Yu. Tolstyakov, A.Yu. Yashin, Nucl. Fusion, **59** (9), 096026 (2019). DOI: 10.1088/1741-4326/ab2cdf
- [30] A.Y. Yashin, A.M. Ponomarenko, N.S. Zhiltsov, K.A. Kukushkin, G.S. Kurskiev, V.B. Minaev, A.V. Petrov, Yu.V. Petrov, N.V. Sakharov, Tech. Phys. Lett., **49** (3), S239 (2023). DOI: 10.1134/S1063785023900893

- [31] A. Yashin, N. Teplova, G. Zadvitskiy, A. Ponomarenko, *Sensors*, **22** (23), 9441 (2022). DOI: 10.3390/s22239441
- [32] V.V. Bulanin, E.Z. Gusakov, V.K. Gusev, G. Zadvitskiy, C. Lechte, S. Heuraux, V.B. Minaev, A.V. Petrov, Yu.V. Petrov, N.V. Sakharov, N. Teplova, A.Yu. Yashin, *Plasma Phys. Rep.*, **46** (5), 490 (2020). DOI: 10.1134/S1063780X20050025
- [33] A. Yashin, V. Bulanin, A. Petrov, A. Ponomarenko, *Appl. Sci.*, **11** (19), 8975 (2021). DOI: 10.3390/app11198975

*Translated by D.Safin*